ACS APPLIED MATERIALS & INTERFACES

Research Article

www.acsami.org

Evolution of AgX Nanowires into Ag Derivative Nano/microtubes for Highly Efficient Visible-Light Photocatalysts

Won San Choi,*[,†] Gyo Yeon Byun,[†] Tae Sung Bae,[‡] and Ha-Jin Lee*[,‡,§]

[†]Department of Chemical and Biological Engineering, Hanbat National University, San 16-1, Dukmyoung dong, Yuseong-gu, Daejeon, 305-719, Republic of Korea

[‡]Jeonju Center, Korea Basic Science Institute, 664-14, Dukjindong 1-ga, Dukjin-gu, Jeonju, 561-756, Republic of Korea

[§]Department of Chemistry, Chonbuk National University, 664-14, Dukjindong 1-ga, Dukjin-gu, Jeonju, 561-756, Republic of Korea

Supporting Information

ABSTRACT: Our study proposes a novel strategy for the synthesis of Ag derivatives (AgX@Ag (X = Cl and Br) or Ag nano/microtubes) using the controlled chemical reduction or electron-beam irradiation of AgX nanowires (NWs), which are formed from the controlled dewetting of a AgX thin film on colloidal particles. The size of the AgX@Ag and Ag nano/microtubes can be controlled using the AgCl NWs as templates and varying the concentration of NaX. By controlling the concentration of NaBr, heterojunction-structured AgCl/AgBr NWs (H-AgCl/AgBr NWs) can be produced from the AgCl NWs due to a partial ion-exchange reaction (low concentration), and the AgBr NWs produced after a complete ion-exchange reaction between Cl- and Br- are further grown into micrometer-sized AgBr wires (high concentration). The resulting AgX NWs can be transformed into corresponding AgX@Ag or Ag nano/microtubes via a controlled chemical or physical method. The AgX derivatives (AgX@Ag nanotubes (NTs) and AgX NWs) are tested as visible-light-induced photocatalysts for decomposition of methyl orange. The AgX@Ag NTs exhibit the best photocatalytic activities due to the advantages of the core@shell structure, allowing multiple reflections of visible light within the interior cavity, providing a well-defined and clean Ag/AgX interface, and preventing direct adsorption of pollutants on AgX because of the shell structure. These advantages allow AgX@Ag NTs to maintain high catalytic performance even after multiple uses. The approach can also be used as a direct method for preparing Ag nano/microtubes with a tailored size and as a new method for incorporating a AgX NW core into a Ag nano/microtube shell. Our approach is useful for synthesizing various types of one-dimensional heterostructured NWs or metal NTs with controlled structures and properties.

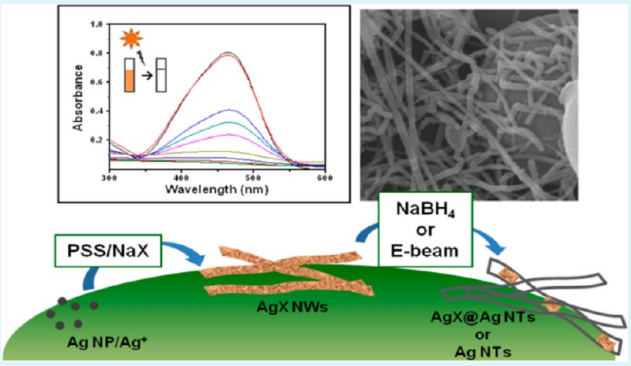

KEYWORDS: *AgX nanowire, AgX@Ag nanotube, Ag nanotube, polyelectrolytes, nanoparticles, photocatalysts*

INTRODUCTION

Visible-light-driven photocatalysts have been an attractive research field because of their high utilization efficiency for solar energy. To effectively use the visible light that comprises 43% of sunlight, efforts have been devoted to designing photocatalysts for high absorption coefficients in the visible and NIR regions.[1−5] As a result, silver halide (AgX)/Ag nanocomposites have been recently developed and are considered new visible-light photocatalysts. Plasmonic nanoparticles (NPs) are more resistant to degradation and exhibit a high absorption coefficient in a broad visible−NIR range.[6−10] However, most nanocomposites have a simple structure that is spherical or dot-shaped,[1−3] and the interface between plasmonic NPs and semiconductor photocatalysts is not well-controlled,[11,12] resulting in decreased efficiency for light absorption and charge separation and transport in semiconductor photocatalysts. Alternatively, if a semiconducting photocatalyst can be selectively or partially converted to plasmonic metals in situ and possesses a favorable structure for enhancing light absorption, the absorption coefficient of the resulting nanocomposites in the visible region can be remarkably enhanced, and the metal/semiconductor interfaces can be clean and well-defined.

Much attention has been focused on one-dimensional (1D) structures involving nanowires (NWs) and nanotubes (NTs) because of their novel properties and potential applications in electronics, photonics, and catalysis.[13−17] Recently, Ag/AgCl (core/shell) NWs, AgBr NWs, and Ag/AgX-decorated titanate NWs with uniform structure have been synthesized at room temperature, which exhibit excellent photocatalytic performance for decomposition of methylene orange under visible-light irradiation.[4,18,19] AgCl/Au NW exhibiting enhanced absorption

Received: August 19, 2013
Accepted: October 14, 2013
Published: October 14, 2013

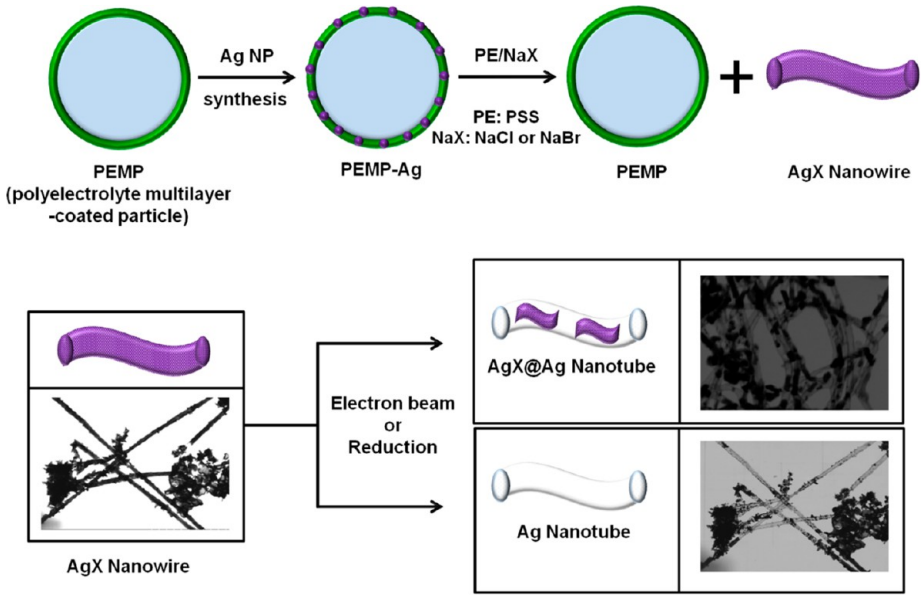

Figure 1. Schematic depiction of the synthesis of Ag derivatives (AgX@Ag (X = Cl and Br) or Ag nano/microtubes) using the controlled chemical reduction or electron-beam irradiation of AgX nanowires, which are formed from the controlled dewetting of a AgX thin film on colloidal particles. The PEMP-Ag still posses a certain amount of Ag ions even after synthesis of AgNPs. These Ag ions within the PEMP-Ag react with incoming NaX to form AgX, which further reacts with PSS to form AgX nanowires. The AgX@Ag nanotubes are used as visible-light-driven photocatalysts.

coefficient in the visible region and enhanced chemical stability has been also reported.[20] Among them, 1D heterostructured NW (1D-HNW) have recently become of particular interest because their functions can be controlled or enhanced by combing a core and shell with different properties.[21,22] However, most of these structures have been fabricated using template strategies involving the preparation of shell layers on preformed core materials. These methods often have limitations in terms of the selection of materials, which must be compatible with the next layer for each successive coating.[23,24] Incompatible structures between a core NW and a shell NW usually result in incomplete coverage, nonuniformity, and structural weakness, which can restrict their future applications.[25−27] In addition, if such a 1D HNW is used as an inside core NW within a shell NW, called a core@shell NW, it is possible that novel properties could be conferred to the resulting structure, based on the nature of the core material because the use of hollow or rattle-typed structures provides a new opportunity to explore advanced materials.[28−34] Thus, the exploration of a novel fabrication strategy for 1D HNWs, enabling the simple production of the core@shell NW structure with good compatibility between the core and shell layers would constitute significant progress in the field.

Above-mentioned expectations led us to develop a new silver halide-based photocatalyst, namely AgX NW within Ag NTs (AgX@Ag) via the controlled reduction or electron beam irradiation of AgX NW formed from the controlled-dewetting of an AgX thin film on colloidal particles.

EXPERIMENTAL SECTION

Materials. Melamine-formaldehyde (MF) particles (1.98 μm, 10 wt %) were purchased from Microparticles GmbH. Poly(sodium 4-styrenesulfonate) (PSS, M_w = 70 000), poly(allylamine hydrochloride) (PAH, M = 15 000), NaCl, NaBr, $AgNO_3$ methylene orange (MO), methylene blue (MB), and $NaBH_4$ were purchased from Aldrich and used as received. Deionized (DI) water with a resistance of 18.2 MΩ cm was obtained using a Millipore Simplicity 185 system.

Preparation of the PEMP(MF/PSS/PAH). A PSS solution (2 mL, 2 mg/mL) was added to 0.13 mL of an aqueous suspension of positively charged MF particles. The dispersion was agitated vigorously on a shaking apparatus for 15 min to allow the PSS to be adsorbed onto the amine groups of the MFs. The dispersion was centrifuged at 10 000 rpm for 2 min, the supernatant was removed, and 2 mL of water was added. This rinsing step was repeated three times. After adsorption of the PSSs on the MF templates, 2 mL of a PAH solution (2 mg/mL) was added to an aqueous suspension of the PSS-coated MF. The dispersion was agitated vigorously on a shaking apparatus for 15 min, and the PEMPs were collected after rinsing three times with water.

Preparation of AgX Nanowires (AgX NWs, X = Cl or Br). An aqueous solution of $AgNO_3$ (2 mL, 0.01 g/1 mL) was added to a suspension of the resulting PEMPs. The dispersion was agitated vigorously on a shaking apparatus for 4 h to allow adsorption of the Ag ions on the PEMPs. This rinsing step was repeated three times. The AgNPs were generated on the surface of the PEMPs by treatment with a 1.6 mM $NaBH_4$ solution for 30 min. After formation of the PEMP-AgNPs, the resulting particles were redispersed in a 2 mL of NaX (X = Cl or Br) solution (0.5 M) containing the PSS (2 mg/mL) for 15 minutes to synthesize the AgX (AgCl or AgBr) NWs. The rinsing step was repeated three times with water. To prepare the heterojunction-type AgCl/AgBr NWs (H-AgCl/AgBr NWs), AgBr submicrowires, and AgBr microwires, the resulting AgCl NWs were redispersed in 2 mL of NaBr solution (0.5, 1, and 2 M, respectively) containing the PSS (2 mg/mL) for 12 h. The rinsing step was repeated three times with water.

Preparation of AgX@Ag and Ag Nanotubes (NTs). To prepare AgX@Ag and Ag NTs, the AgCl NWs were repeatedly treated (2 and 5 times, respectively) with a 2 mL of a $NaBH_4$ (1.6 mM) solution. The rinsing step was repeated three times.

Photocatalytic Activity of AgX Nanowires and AgX@Ag Nanotubes. The catalysts (AgX nanowires or AgX@Ag nanotubes containing the PEMPs) (10 mg) were added to an aqueous solution (20 mL) of MO molecules (10 mg/L). The amount of catalyst excluding the PEMPs was calculated based on the weight difference after removal of the PEMPs by calcination at 500 °C for 4 h, and the amount was determined to be approximately 1 mg. The mixture was stored in the dark for 30 min to reach an adsorption−desorption equilibrium of MO molecules on the catalysts. The solution was then

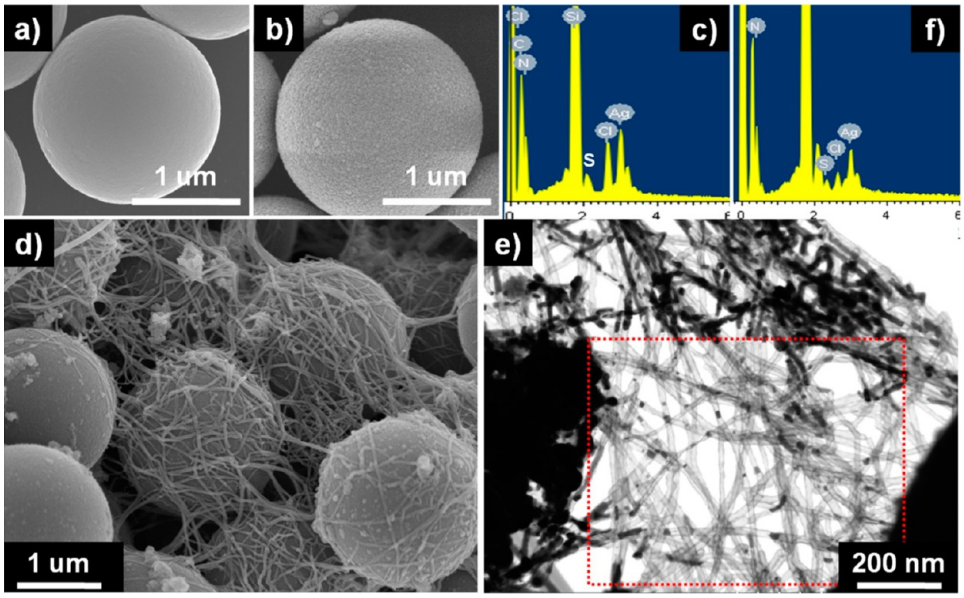

Figure 2. Electron microscopy images and associated EDX data. SEM images of PEMPs (a) before and (b) after synthesis of AgNPs (PEMP-AgNP). (c) EDX data of b. (d) SEM image of the PEMP-AgNP after PSS/NaCl treatment for 15 min (PEMP-AgNP/PSS+NaCl(0.5 M)). (e) UHR-SEM image of d, revealing nanotubes and nanowires in the irradiated and non-irradiated FEB regions, respectively. The red box highlights the irradiated region. f) EDX data of the irradiated FEB region in e. The concentration of NaCl used in this study was 0.5 M.

exposed to a 300 W Xenon lamp (XLS-300P, Spectro). To eliminate the decomposition effect of MO from the Xe lamp itself, the distance between the catalyst solution and the lamp was maintained at 3 meters. The distance was determined after confirming that the decomposition of MO without catalysts was negligible under the Xe lamp for 30 min. Aliquots of solution (1 mL) were removed from the reaction system at various times. Each sampling solution was centrifuged at 10 000 rpm for 5 min to separate the catalyst. The top solution was transferred to a quartz cuvette to take the absorption spectrum. The reactions were performed under constant magnetic stirring at room temperature.

Characterization. UHR- and FE-SEM/EDX data were obtained using Hitachi S-5500 and S-4700 microscopes operated at 30 kV and 10 kV, respectively. XRD patterns were obtained using a Rigaku X-ray diffractometer equipped with a Cu Kα source. UV−vis absorption spectra were recorded on a UV−vis spectrophotometer (Scinco Evolution 201).

RESULTS AND DISCUSSION

Figure 1 shows a synthetic scheme of Ag derivatives (AgX@Ag (X = Cl and Br) or Ag nano/microtubes) using the controlled chemical reduction or electron-beam irradiation of AgX nanowires (NWs), which are formed from the controlled dewetting of a AgX thin film on colloidal particles. The polyelectrolyte multilayer-coated particles (PEMPs), MF/PSS/PAH, were prepared by coating poly(styrene sulfonate) (PSS) and poly(allylamine hydrochloride) (PAH) onto positively charged melamine-formaldehyde (MF) particles. Ag ions can be adsorbed within the PEMs consisting of PSS and PAH. Primary amine groups possessing unshared electron pairs of PAH as well as negative charges of PSS can provide reaction sites for adsorption of Ag ions. After synthesis of AgNPs on the PEMPs by chemical reduction metnod, PEMP-AgNPs were used as templates for preparing Ag derivative NWs and NTs.

Images a and b in Figure 2 present scanning electron microscope (SEM) images of the PEMPs before and after synthesis of AgNPs, respectively. After the synthesis of the AgNPs, the surface morphology of the PEMPs became slightly rough. Energy-dispersive X-ray (EDX) data confirmed the formation of the mixture of AgNPs and AgCl on the PEMPs (Figure 2c). During the adsorption of Ag precursors on the PEMPs, one portion of the Ag precursors can be reacted with Cl ions of PAH to form the AgCl. After treatment of the resulting particles (PEMPs) with PSS dissolved in a 0.5 M NaCl solution, surprisingly, NWs with widths between 30 and 110 nm and lengths of several tens of micrometers were observed on the surface of the PEMP-AgNPs (Figure 2d). The EDX and X-ray diffraction (XRD) data of the resulting products indicate that the NWs are composed of silver chloride (AgCl), and the results will be discussed in detail below. Ultra-high-resolution SEM (UHR-SEM) measurements were performed to investigate the structure of the AgCl NWs. A very interesting phenomenon was observed upon focused electron beam (FEB) irradiation for the SEM measurement. The AgCl NWs were observed in the non-irradiated FEB region, whereas NTs were observed in the irradiated FEB region (red box in Figure 2e). Because of the in situ observation, AgCl is thought to have migrated to both ends of the NWs and disappeared upon e-beam irradiation (see Figure S1 in the Supporting Information). Actually, both the EDX peaks of Ag and Cl were detected before and after FEB irradiation of the AgCl NWs; however, the intensity of the Cl peak remarkably decreased after FEB irradiation compared with that of the Ag peak (Figure 2c, f). It has been reported that the e-beam irradiation on AgCl results in the decomposition of AgCl into Ag^0 with removal of Cl_2,[35] and the e-beam has been used for the reduction of metal precursors into the corresponding metals.[36] Moreover, volume reduction of the NTs was observed when the NW structure was transformed into a NT one after FEB irradiation, which was a result of the density difference between AgCl (5.56 g/cm^3) and Ag (10.49 g/cm^3) (see Figure S1 in the Supporting Information). The results above suggest that the AgCl NWs are partially converted into Ag NTs under FEB irradiation. Notably, Ag NTs as well as AgCl@Ag NTs (AgCl core in Ag shell) were obtained by varying the e-beam irradiation dose (Figure 2e and Figure S2 in the Supporting Information). More

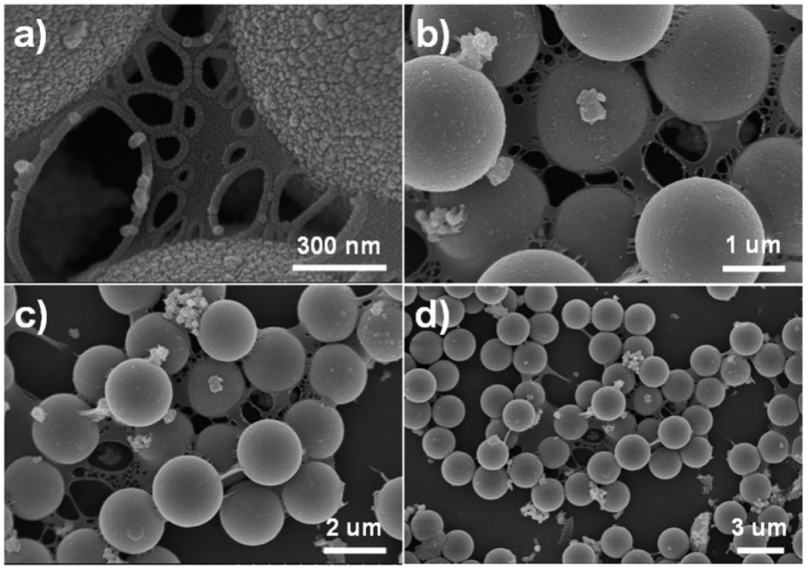

Figure 3. SEM images of PEMP-AgNPs after 1 min of PSS/NaCl treatment ((a–d) high to low magnification), illustrating the formation process of the nanowires evolved from peeled thin layers via peeling, rolling, and elongating the thin layers. (a) AgNPs are observed on the peeled layer between the PEMP-AgNPs. (b–d) Process exhibiting transformation of sheet structure into short wire structure.

details on the transformation of AgCl NWs into Ag NTs will be discussed with the XRD results.

To investigate the formation mechanism of the AgCl NWs produced by PSS/NaCl treatment of PEMP-AgNPs, we separately added PSS or NaCl to the PEMP-AgNPs. When adding PSS only, no particular phenomenon was observed on the surface of the PEMP-AgNPs (see Figure S3a in the Supporting Information). However, the addition of NaCl resulted in the formation of the expected AgCl but not a wire structure (see Figure S3b, i in the Supporting Information). It is well-known that Ag ions easily react with NaCl to form AgCl.[1−3] In addition, our reduction condition partially reduces Ag precursors to Ag NPs, thus preserving the Ag ions to form AgCl upon the addition of NaCl. This mechanism becomes clearer using the following experiment. For the complete reduction of Ag precursors, no AgCl was formed even if NaCl was added (see Figure S3c, j in the Supporting Information). Notably, the reaction of Ag ions and NaCl in the absence of a reduction process did not effectively form AgCl NWs. The PSS/NaCl treatment of Ag ion-loaded PEMPs (PEMP-Ag^+), in which the reduction process was not performed, led to the formation of primarily AgCl particles with an extremely small amount of AgCl NWs (see Figure S3d in the Supporting Information). Therefore, in the absence of a reduction process (without AgNPs), the AgCl NWs were directly transformed to irregular-shaped Ag NWs (not tubes), and the structures were degraded upon FEB irradiation (see Figure S4 in the Supporting Information). In the presence of Ag NPs synthesized via partial reduction, the NTs began to form from the AgCl NW surface with the AgNPs, and Cl_2 gas was removed by FEB irradiation (see Figures S2b and S5 in the Supporting Information). Considering that AgNPs were formed by partial reduction and their position on the AgCl NWs, it can be deduced that when the AgCl NWs transform into the Ag NTs with the removal of Cl_2 gas by FEB irradiation, the AgNPs existing on the AgCl nanowires play an important role as seeds for the growth of reduced Ag as Ag nanotubes at the surface of the AgCl NWs. Although the major reason for the mass production of the AgCl NWs from the presence of AgNPs has not yet been clearly identified, it is clear that the presence of partially reduced AgNPs on the PEMP or AgCl NW surfaces is necessary for the mass production of NWs or NTs, respectively (see Figures S4 and S5 in the Supporting Information).

The role of polyelectrolyte (PEs) was also investigated to elucidate the mechanism. The use of polyacrylic acid (PAA)/NaCl (or PAH/NaCl, which will be discussed later) instead of PSS/NaCl led to the formation of only AgCl particles (see Figure S3e in the Supporting Information). This result indicates that NaCl primarily assists in the formation of AgCl particles and that the PSS in the NaCl solution induces the formation of the wire-shaped structure rather than a particle-shaped structure. In the absence of PEMs (PSS(−)/PAH(+)), an extremely small amount of NWs was observed, which implies that the PEMs acted as a reservoir for Ag ions to react with NaCl to form AgCl NWs (see Figure S3f in the Supporting Information).[34] However, no further remarkable growth of the NWs was observed even if the number of PEM layers (more than 3) was increased. In summary, it is expected that the PSS form complexes with the AgCl nucleuses formed within the PEMs, the Ag ions react with NaCl, and the complexes transform into a wire shape as the reaction proceeds. Indeed, the UHR-SEM/EDX data revealed that the AgCl NWs contain small amounts of sulfur originating from the PSS (Figure 2c, f). Moreover, among the PEs, considering the wire-shaped structure formed by only the PSS, the formation mechanism of the NWs can be attributed to the characteristics of PSS as a surfactant, forming micelles or emulsifying matter at certain concentrations.[37,38] At PSS concentrations higher or lower concentration than 2 mg/mL, no NWs were formed (see Figure S3g, h in the Supporting Information).

To investigate the effect of PSS on the formation of the NWs, we investigated the evolution of the NWs. Figure 3 shows the SEM images of the PEMP-AgNPs after 1 min of PSS/NaCl treatment. A thin layer connecting the particles (PEMP-AgNPs) was peeled from the surface of the PEMP-AgNPs and elongated into rods (short wires). The width of the elongated rod was similar to that of the AgCl NWs, and rods of

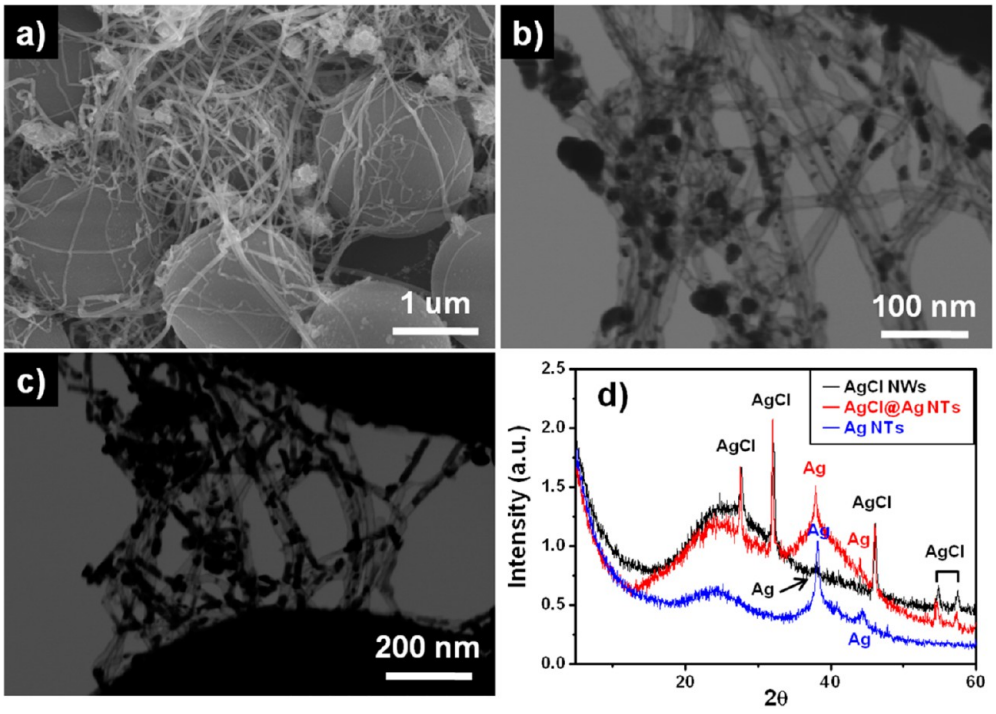

Figure 4. (a) SEM image of the Ag NTs prepared from AgCl NWs after 5 treatments with a low concentration of $NaBH_4$ (1.6 mM). (b) UHR-SEM image of a. The black regions signify metallic Ag. (c) UHR-SEM image of AgCl@Ag NTs prepared from AgCl nanowires after 2 treatments with a low concentration of $NaBH_4$ (1.6 mM). The black regions signify AgCl. A well-defined and cleaned Ag/AgX interface is observed. (d) XRD data of b (Ag NTs), c (AgCl@Ag NTs), and AgCl NWs.

1−2 μm were frequently observed. EDX data confirmed that the rods were composed of AgCl. The NW shape began to grow after 5 min (see Figure S6a in the Supporting Information). After 1 h, the NWs were similar in length and width to the NWs obtained after the reaction for 15 minutes (see Figure S6b in the Supporting Information). PAH/NaCl and PAA/NaCl were used instead of PSS/NaCl and were separately treated for 1 minute and 1 h. In both cases, dewetting (particle formation) of AgCl resulting from the NaCl was observed, revealing the rupture of the AgCl thin film and the formation of AgCl droplets on the PEMP-AgNPs (see Figure S6c−f in the Supporting Information). However, the peeled thin layers or NWs observed when the PEMP-AgNPs were treated with PSS/NaCl were not observed under these conditions. Notably, a portion of the AgNPs was detached when the thin layers that contained the AgNPs were peeled from the PEMP-AgNPs (Figure 3a). Considering that the AgNPs attached to the NW surface (see Figure S5 in the Supporting Information), this result suggests a transformation of the thin layers into NWs during the PSS/NaCl treatment. On the basis of the above results, we propose a plausible mechanism for the formation. The PSS acts as a surfactant and emulsifies the AgCl, prevents dewetting of the AgCl (prohibition of particle formation), and disperses the AgCl as a thin layer on the PEMP-AgNPs as the PSS forms complexes with AgCl. Finally, the AgCl emulsified by the PSS is removed as a thin layer from the PEMP-AgNPs and then is transformed and grows into the NW form because of the spherical geometry of the templates. Use of a planar template instead of the spherical PEMPs resulted in the formation of irregular-shaped structures, not NWs, which implies that the geometry of the template affects the formation of the NWs (see Figure S7 in the Supporting Information). Meanwhile, the effects of the NaCl concentration and reaction time on the growth of the AgCl NWs were not significant (see Figure S8 in the Supporting Information).

Transformation of the AgCl NWs into Ag nanotubes by FEB irradiation was observed in the TEM images. However, the e-beam method, which employed a limited area of irradiation, would not be useful for broad applications or mass production. Thus, we attempted to find other methods for large-scale, facile production. We confirmed that AgCl nanowires can be easily converted to Ag or AgCl@Ag NTs using a chemical method. When a high concentration of the reducing agent was used, the NW structures were partially degraded due to a sudden release of an abundance of Cl_2 gas and were not transformed into NTs even after prolonged FEB irradiation (see Figure S9 in the Supporting Information). It appears that the AgCl NWs were directly transformed to Ag NWs (not tubes) because of the high dose of the reducing agent. However, when a low concentration of the reducing agent was repeatedly used until the reduction was completed (5 times), NTs with no noticeable damage to their external appearance were obtained (Figure 4a). No further structural changes of the Ag NTs were observed even after FEB irradiation, and a small quantity of Ag particles was formed inside or outside the Ag NTs (Figure 4b). The X-ray diffraction (XRD) patterns clearly show Ag peaks without AgCl peaks after 5 reductions compared with the AgCl NWs before the reduction, proving the complete transformation of AgCl NWs into Ag NTs (black and blue lines, Figure 4d). A very weak Ag peak was observed in the AgCl NWs before the reduction due to the presence of AgNPs on the AgCl NW surface (black line). Notably, incomplete reduction (twice) led to the formation of a NT intermediate such as AgCl@Ag NTs (AgCl core-in-Ag shell), which could be further converted into Ag NTs by FEB irradiation (Figure 4c). A certain amount of

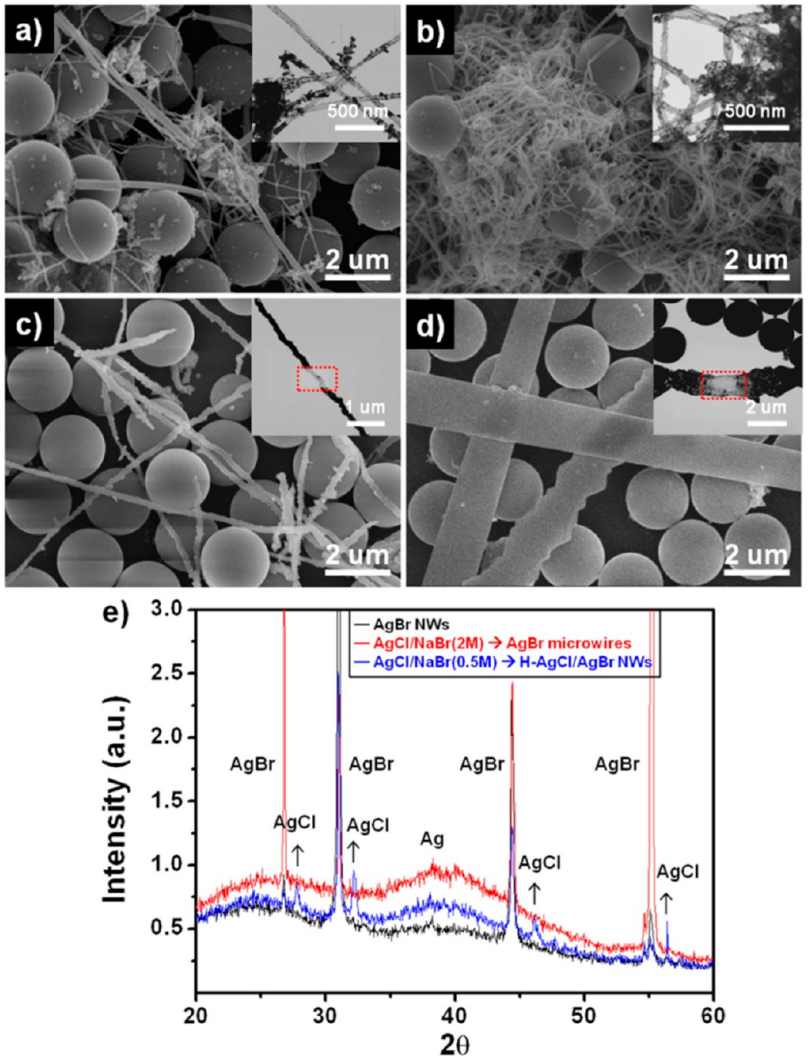

Figure 5. (a) SEM image of AgBr NWs on the PEMPs (PEMP-AgNP/PSS+NaBr (0.5 M, 15 min.)). SEM image of (b) H-AgCl/AgBr NWs, (c) AgBr sub-MWs, and (d) AgBr MWs prepared from the AgCl NWs via an ion-exchange reaction with (b) NaBr (0.5 M), (c) NaBr (1 M), and (d) NaBr (2 M) for 12 h, respectively. PEMP-AgNP/PSS+NaCl(0.5 M)/PSS+NaBr ((b) 0.5, (c) 1, and (d) 2 M). The insets for a and b show Ag NTs obtained from the AgBr and H-AgCl/AgBr NWs , respectively, via chemical reduction. The insets for c and d show the corresponding Ag tubes formed within the selected area by FEB irradiation. (e) XRD data of AgBr NWs (black line), H-AgCl/AgBr NWs (blue line), and (red line) AgBr MWs.

AgCl randomly migrated to outside of Ag NTs and it formed metallic Ag clusters (Figure 4c and Figure S10 in the Supporting Information). The rest of AgCl was still remained within the Ag NTs, which was used as photocatalysts. Although the distribution of the remained AgX within the Ag NTs was irregular because of random reduction of AgX by $NaBH_4$, most of AgXs within the Ag NTs were well covered with Ag NTs (Figure 4c and Figure S10 in the Supporting Information). These phenomena were frequently observed in almost all areas. Instantaneous high energy of FEB resulted in migrating AgCl into ends of the NTs, evaporating Cl_2 gas, and forming pure Ag NTs without Ag clusters within the NTs (see Figure S1 in the Supporting Information). However, such pure Ag NTs were not formed by chemical reduction method because the AgCls were randomly reduced to metallic Ag with time gap by $NaBH_4$. As a result, the Ag and AgX@Ag NTs containing randomly distributed metallic Ag were obtained by complete (5 times) and incomplete (2 times) reduction conditions, respectively. The presence of AgCl@Ag NTs prepared by partial chemical reduction was confirmed by XRD analysis. The intensities of the Ag peaks noticeably increased after the second reduction compared to those of the AgCl NWs, and the AgCl peaks were still present because of the incomplete reduction (black and red lines, Figure 4d). These results indicate that our approach can be used as a direct and facile method for the mass production of AgCl NW, AgCl@Ag NTs, and Ag NTs.

To further confirm our hypothesis for the mechanism of AgX NW synthesis, we evaluated the morphology of other silver halides and derivatives prepared by the same protocol with AgCl NWs. Figure 5a shows AgBr NWs with widths of 80 to 250 nm, which is almost double the size of the AgCl NWs. These NWs can be transformed into Ag NTs or AgBr@Ag NTs by complete or partial (including FEB irradiation) chemical reduction, respectively (inset of Figure 5a and Figure S11 in the Supporting Information). According to our additional study, other AgX NWs (X = F and I) were not formed. Notably, heterojunction-type AgCl/AgBr NWs (H-AgCl/AgBr) could also be prepared in the presence of AgCl NWs on PEMP-AgNPs (Figure 5b and blue line in Figure 5e). Treatment of the PSS/NaBr on the AgCl NWs resulted in the formation of H-

AgCl/AgBr NWs via an ion-exchange reaction between the AgCl NWs and NaBr. Notably, as the concentration of NaBr increases (0.5−2 M), the Cl ions within the AgCl NWs became gradually substituted with Br ions, leading to the formation of H-AgCl/AgBr NWs and AgBr microwires (Figure 5b−e and Figure S12 in the Supporting Information). All of the AgXs were identified by XRD analysis (JCPDS, 01-085-1355/00-006-0438). At low concentrations of PSS/NaBr (0.5 M), even though the content of AgCl decreased by 20% within the H-AgCl/AgBr NWs compared with the AgCl NWs, the NWs were still approximately the same size as the AgCl NWs (Figure 5b and Figure S12 in the Supporting Information). At a high concentration of PSS/NaBr (1-2 M), however, submicro- or microwires were formed instead of NWs, and the gradual growth of the AgBr wires was a function of the increasing concentration of NaBr (Figure 5c, d). The EDX and XRD data suggest that the AgCl NWs were completely transformed into AgBr microwires (Figure 5e and red line in Figure S12 in the Supporting Information). The characteristics of the structural changes into Ag NTs, which were observed in AgCl upon FEB irradiation or chemical reduction, were still observed in the AgBr NWs, H-AgCl/AgBr NWs and AgBr microwires (insets of Figure 5). Meanwhile, the AgBr wires prepared in the absence of AgCl NW templates using a high concentration of NaBr (PSS+NaBr(2 M)) exhibited network structures, which were completely different from the AgBr wire structures synthesized from AgCl NWs using the ion-exchange reaction (see Figure S13 in the Supporting Information). Furthermore, the AgBr prepared from AgCl exhibited a different crystal growth pattern, including different intensities at certain planes of the AgBr crystals, compared with the AgBr prepared without AgCl templates (black and red lines, Figure 5e). This result suggests that growing AgBr on AgCl NW templates follows a different growth mechanism compared with the direct growth of AgBr on PEMP-AgNPs. Based on these observations, a possible formation mechanism of the AgBr microwires has been proposed. At a low concentration of NaBr, H-AgCl/AgBr NWs without changing size can be formed from AgCl NWs through a partial ion-exchange reaction. However, at a high concentration of NaBr, the AgCl completely transforms into AgBr NWs after a complete ion-exchange reaction, and the AgBr NWs further grow to micrometer-sized AgBr wires. Hence, the AgBr microwires synthesized in the presence or absence of AgCl NWs exhibit a different crystal growth pattern, which could lead to a variation in properties.

The photocatalytic activities of the AgX NWs and their derivatives were evaluated based on the decomposition of methyl orange (MO) under visible-light irradiation at room temperature. Because the performance differences of various sized NWs produced by varying the concentration of NaX (0.5 - 2 M) were not significant (green and blue dots, Figure 6a), primarily the photocatalytic activities of the AgX NPs, AgX NWs, and AgX@Ag NTs prepared using NaX (0.5 M) were investigated. The catalytic activities were tested without separation of the PEMP templates. The amount of the catalysts used was approximately 1 mg, which was calculated based on the weight difference after removing the PEMP templates, and this was very small amount compared with the reported values.[1−4] All of the AgX NWs clearly exhibited excellent photocatalytic activities compared with the AgX NPs (Figure 6a and Figure S14 in the Supporting Information). However, in the absence of catalysts, only 11% of MO dye was decomposed during 30 min and it took over 6 h to nearly completely

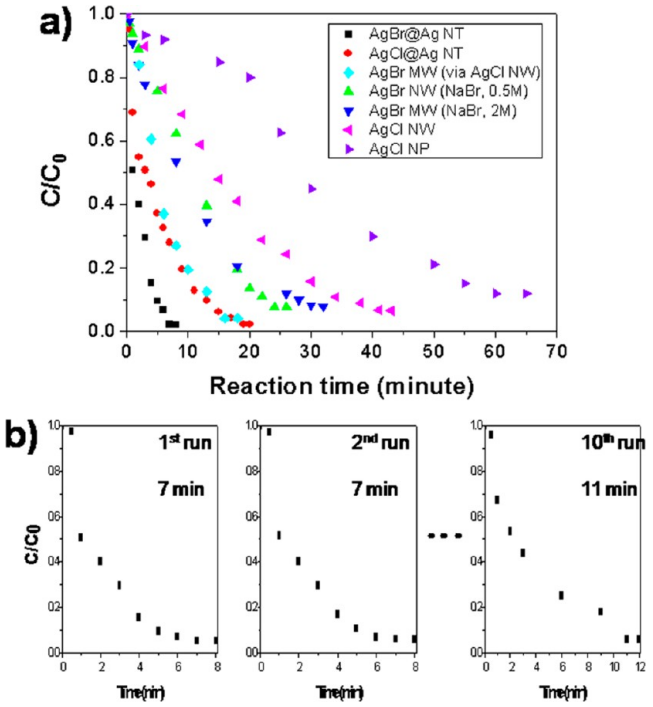

Figure 6. (a) Degradation of MO molecules catalyzed with various AgX NWs and AgX@Ag NTs under visible-light irradiation. The absorbances at 464 nm were used for plotting. (b) Results from recycling the AgBr@Ag NTs.

decompose MO dye (see Figure S15 in the Supporting Information). Detailed photocatalytic reaction can be found in the Supporting Information (Figures S14). The AgBr NWs exhibited better performances than the AgCl NWs and could completely decompose the MO within 24 minutes after light irradiation due to rapid combination with holes (green vs. magenta dots, Figure 6a).[39] Notably, the AgBr microwires obtained from the AgCl NWs exhibited a much better performance than the directly grown AgBr nano- or microwires (light blue vs green/blue dots). We assume that the AgBr molecules are rearranged during the ion-exchange reaction and regrow, as confirmed in the XRD data, which is favorable for the photocatalytic decomposition of the MO. Furthermore, the AgX@Ag NTs exhibited significantly higher catalytic performances than the AgX NWs (black/red dots vs. green/magenta dots), and in particular, AgBr@Ag exhibited the highest performance among the nano- or microwires (black dots). We believe that the outstanding performance of the AgX@Ag NTs result from the advantages of the core@shell structures. (I) Their unique structures with appropriate inner spaces could allow multiple reflection of incident visible light within the interior cavity, allowing more efficient use of the light source, thus offering improved catalytic activity. In fact, the AgX@Ag NTs exhibited stronger absorption in the visible region compared with the AgX NWs or the Ag NTs (see Figure S16 in the Supporting Information). Analogous study further supports our results. It has been recently demonstrated that multilight-reflection caused by light confinement within the hollow structure enables catalysts to efficiently use incident light without loss.[40] (II) Core@shell structures, where the core (AgX NW) is well covered with a shell as a protector (Ag NT), could provide a well-defined and clean Ag/AgX interface (Figures 2e and 4c), (II-a) enhancing the interfacial charge transfer and preventing the electron-hole from recombination,

as well as (II-b) preventing adsorption of pollutants onto the AgX as a result of the shell structures. (II-a) In fact, because AgNPs are randomly formed on the AgX surface, the AgX NWs possess a less well-defined Ag/AgX interface, leading to a lower catalytic activity than that of AgX@Ag NTs (black vs. green/red vs. purple in Figure 6a). (II-b) Generally, the strong adsorption of pollutants on a catalyst surface is not favorable for the catalytic efficiency and stability of the catalysts.[20,41] Spectral analysis indicates that almost no MO molecules (negative charges) are adsorbed onto the AgBr@Ag NTs, whereas 3% of the MO molecules are adsorbed onto AgBr NWs in a few minutes even with the same charges (see Figure S17a in the Supporting Information). Meanwhile, in the presence of positively charged methylene blue (MB), 30 and 45% MB adsorption was observed for AgBr@Ag NTs and AgBr NWs, respectively. Considering that 28% MB adsorption on negatively charged PEMP templates was observed, a 30% MB adsorption by AgBr@Ag NTs on the PEMPs is negligible (2% of MB adsorption on AgBr@Ag NTs) compared with the 17% MB adsorption on AgBr NWs (see Figure S17b in the Supporting Information). This result suggests that the metal shell (Ag NT) plays a key role in preventing the adsorption of ionic pollutants regardless of the charges. Another remarkable advantage of the core@shell structures is that the aggregation of cores after the reaction, which is generally observed in catalytic NPs, can be effectively avoided by the shell structures, offering enhanced catalytic efficiency. To verify that high catalytic performance was retained, decomposition experiments of MO using AgBr@Ag NTs were performed up to 10 times. We observed that the MO molecules were rapidly decomposed after every injection of the MO solution, and the AgBr@Ag NTs were stable and showed a nearly constant decomposition rate (Figure 6b). After the 10^{th} use, the rate decreased slightly. However, for the AgBr NWs, the decomposition rate decreased remarkably after the 3rd use (see Figure S18 in the Supporting Information). FE-SEM images of the AgBr NWs after three uses clearly reveal that Ag aggregates were formed from the degradation of the AgBr NWs (see Figure S19a, b in the Supporting Information), in contrast to the clean surfaces of the AgBr@Ag NTs even after ten uses (see Figure S19c, d in the Supporting Information). We believe that the outstanding stability of the AgX@Ag NTs under repeated use is attributed to the core@shell structures, which prevent the decomposition or contamination of AgX.

CONCLUSION

We have demonstrated a novel strategy for the synthesis of Ag derivatives (AgX@Ag or Ag nano/microtubes) using the controlled reduction or electron-beam irradiation of AgX NWs formed from the controlled dewetting of a AgX thin film on colloidal particles. The size of the AgX@Ag and Ag nano/microtubes can be controlled using the AgCl NWs as templates and varying the concentration of NaX. At low and high concentrations of NaBr, heterojunction-structured AgCl/AgBr NWs can be formed from the AgCl NWs via a partial ion-exchange reaction, and the AgBr NWs produced after a complete ion-exchange reaction were further grown into micrometer-sized AgBr wires. The resulting AgX NWs can be transformed into the corresponding AgX@Ag or Ag nano/microtubes via a controlled chemical or physical method. The AgBr obtained from the AgCl NWs exhibited a much higher catalytic performance for the decomposition of methyl orange under visible-light irradiation than the directly obtained AgBr. Thus, using this method, it is possible to induce the rearrangement of AgBr molecules during the ion-exchange reaction and re-growth, which is more favorable for the photocatalytic decomposition of pollutants. Furthermore, AgX@Ag NTs exhibited the best photocatalytic activities because of the presence of a core@shell structure, permitting multiple reflections of visible light within the interior cavity, providing a well-defined and clean Ag/AgX interface, and preventing the adsorption of pollutants on AgX due to the shell structure. These advantages allow AgX@Ag NTs to maintain high catalytic performance even after multiple uses (more than ten times). The approach can also be used as a direct method for preparing Ag nano/microtubes with tailored size and as a new method for incorporating an AgX NW core into an Ag nano/microtube shell. We believe that this novel approach would be useful for synthesizing various types of one-dimensional heterostructured NWs or metal NTs with controlled structures and properties.

ASSOCIATED CONTENT

Supporting Information

UHR-SEM images of AgCl NWs, SEM images of PEMP-AgNPs or -Ag^+/PSS, NaCl, or PSS/NaCl, enlarged SEM image of the AgCl NWs, SEM image of PEM film-AgNP/(PSS/NaCl), SEM images of PEMP-AgNP/PSS+NaCl(2 M) and PEMP-AgNP/PSS+NaCl/$NaBH_4$(40 mM), UHR-SEM images of AgBr@Ag NTs, EDX of PEMP-AgNP/PSS+NaCl/PSS +NaBr(0.5 M and 2 M), SEM images of PEMP-AgNP/PSS +NaBr(2 M), UV−vis spectral changes of MO molecules, three recycling results of the AgBr NWs, SEM images after reuse of the AgBr NWs and the AgBr@Ag NT. This material is available free of charge via the Internet at http://pubs.acs.org.

AUTHOR INFORMATION

Corresponding Authors

*E-mail: choiws@hanbat.ac.kr.
*E-mail: hajinlee@kbsi.re.kr.

Notes

The authors declare no competing financial interest.

ACKNOWLEDGMENTS

This work was supported by the Korea Basic Science Institute (KBSI) grant T33740 and a grant from the cooperative R&D program funded by the Korea Research Council for Industrial Science and Technology.

REFERENCES

(1) Wang, P.; Huang, B. B.; Qin, X. Y.; Zhang, X. Y.; Dai, Y.; Wei, J. Y.; Whangbo, M. H. *Angew. Chem. Int. Ed.* **2008**, *47*, 7931−7933.
(2) An, C. H.; Peng, S.; Sun, Y. G. *Adv. Mater.* **2010**, *22*, 2570−2574.
(3) Kuai, L.; Geng, B.; Chen, X.; Zhao, Y.; Luo, Y. *Langmuir* **2010**, *26*, 18723−18727.
(4) Bi, Y. P.; Ye, J. H. *Chem.—Eur. J.* **2010**, *16*, 10327−10331.
(5) Wu, C. G.; Chao, C. C.; Kuo, F. T. *Catal. Today* **2004**, *97*, 103−112.
(6) Huang, X.; El-Sayed, I. H.; Qian, W.; El-Sayed, M. A. *J. Am. Chem. Soc.* **2006**, *128*, 2115−2120.
(7) Sun, Y.; Xia, Y. *Analyst* **2003**, *128*, 686−691.
(8) Zhang, Q.; Ge, J.; Pham, T.; Goebl, J.; Hu, Y.; Lu, Z.; Yin, Y. *Angew. Chem., Int. Ed.* **2009**, *48*, 3516−3519.
(9) Tao, A.; Sinsermsuksakul, P.; Yang, P. *Angew. Chem., Int. Ed.* **2006**, *45*, 4597−4601.
(10) Orendorff, C. J.; Sau, T. K.; Murphy, C. J. *Small* **2006**, *2*, 636−639.

(11) Georgekutty, R.; Seery, M. K.; Pillai, S. C. *J. Phys. Chem. C.* **2008**, *112*, 13563−13570.
(12) Yu, J.; Dai, G.; Huang, B. *J. Phys. Chem. C.* **2009**, *113*, 16394−16401.
(13) Duan, X.; Huang, Y.; Cui, Y.; Wang, J.; Lieber, C. M. *Nature* **2001**, *409*, 66−69.
(14) Barth, J. V.; Costantini, G.; Kern, K. *Nature* **2005**, *437*, 671−679.
(15) Lu, W.; Lieber, C. M. *Nat. Mater.* **2007**, *6*, 841−850.
(16) Wu, Y.; Yang, P. *J. Am. Chem. Soc.* **2001**, *123*, 3165−3166.
(17) Xia, Y.; Yang, P. D.; Sun, Y. G.; Wu, Y. Y.; Mayers, B.; Gates, B.; Yin, Y. D.; Kim, F.; Yan, Y. Q. *Adv. Mater.* **2003**, *15*, 353−389.
(18) Bi, Y.; Ye, J. *Chem. Commun.* **2009**, 6551−6553.
(19) Tang, Y.; Jiang, Z.; Deng, J.; Gong, D.; Lai, Y.; Tay, H. T.; Joo, I. T. K.; Lau, T. H.; Dong, Z.; Chen, Z. *ACS Appl. Mater. Interfaces* **2012**, *4*, 438−446.
(20) Sun, Y. *J. Phys. Chem. C* **2010**, *114*, 2127−2133.
(21) Yin, Y.; Lu, Y.; Sun, Y.; Xia, Y. *Nano Lett.* **2002**, *2*, 427−430.
(22) Wu, Y.; Fan, R.; Yang, P. *Nano Lett.* **2002**, *2*, 83−86.
(23) Li, Q.; Wang, C. *J. Am. Chem. Soc.* **2003**, *125*, 9892−9893.
(24) Hua, B.; Motohisa, J.; Kobayashi, Y.; Hara, S.; Fukui, T. *Nano Lett.* **2009**, *9*, 112−116.
(25) Hwang, Y.; Boukai, A.; Yang, P. *Nano Lett.* **2009**, *9*, 410−415.
(26) Ghoshal, T.; Biswas, S.; Kar, S. *J. Phys. Chem. C.* **2008**, *112*, 20138−20142.
(27) Law, M.; Greene, L. E.; Radenovic, A.; Kuykendall, T.; Liphardt, J.; Yang, P. *J. Phys. Chem. B.* **2006**, *110*, 22652−22663.
(28) Choi, W. S.; Park, J.-H.; Koo, H. Y.; Kim, J.-Y.; Cho, B. K.; Kim, D.-Y. *Angew. Chem. Int. Ed.* **2005**, *44*, 1096−1101.
(29) Shchukin, D. G.; Möhwald, H. *Langmuir* **2005**, *21*, 5582−5587.
(30) Kamata, K.; Lu, Y.; Xia, Y. *J. Am. Chem. Soc.* **2003**, *125*, 2384−2358.
(31) Kim, M.; Sohn, K.; Na, H. B.; Hyeon, T. *Nano Lett.* **2002**, *2*, 1383−1387.
(32) Kim, J. Y.; Yoon, S. B.; Yu, J.-S. *Chem. Commun.* **2003**, 790−791.
(33) Gao, C.; Donath, E.; Möhwald, H.; Shen, J. *Angew. Chem. Int. Ed.* **2002**, *41*, 3789−3793.
(34) Choi, W. S.; Koo, H. Y.; Kim, D.-Y. *Adv. Mater.* **2007**, *19*, 451−455.
(35) Goessens, C.; Schryvers, D.; Dekeyzer, R.; Landuyt, J. V. *Electron Microscopy* **1992**, *2*, 649−650.
(36) Pai, Y.-H.; Huang, H.-F.; Chang, Y.-C.; Chou, C.-C.; Shieu, F.-S. *J. Power Sour.* **2006**, *159*, 878−884.
(37) Xiangbing, L.; Zuchen, L.; Jim, C.; Scriven, L. E.; Davis, H. T. *J. Phys. Chem.* **1995**, *99*, 10865−10878.
(38) Kogej, K.; Skerjanc. *Acta Chim. Slov.* **1998**, *45*, 443−453.
(39) Wang, P.; Huang, B.; Zhang, X.; Qin, X.; Jin, H.; Dai, Y.; Wang, Z.; Wei, J.; Zhan, J.; Wang, S.; Wang, J.; Whangbo, M.-H. *Chem.—Eur. J.* **2009**, *15*, 1821−1824.
(40) Tang, Y.; Jiang, Z.; Xing, G.; Li, A.; Kanhere, P. D.; Zhang, Y.; Sum, T. S.; Li, S.; Chen, X.; Dong, Z.; Chen, Z. *Adv. Funct. Mater.* **2013**, *23*, 2932−2940.
(41) Gliman, P. B. *Photogr. Sci. Eng.* **1974**, *18*, 475−478.